Physics Letters A 372 (2008) 5071–5076

Contents lists available at ScienceDirect

Physics Letters A

www.elsevier.com/locate/pla

Finite element method for solving Kohn–Sham equations based on self-adaptive tetrahedral mesh

Dier Zhang [a], Lihua Shen [b], Aihui Zhou [b], Xin-Gao Gong [a,*]

[a] Department of Physics, Fudan University, Shanghai 200433, China
[b] Institute of Computational Mathematics and Scientific/Engineering Computing, Academy of Mathematics and System Sciences, Chinese Academy of Sciences, PO Box 2719, Beijing 100080, China

ARTICLE INFO

Article history:
Received 10 March 2008
Received in revised form 23 May 2008
Accepted 26 May 2008
Available online 5 June 2008
Communicated by R. Wu

PACS:
71.15.-m

Keywords:
Finite element method
Electronic structure calculations

ABSTRACT

A finite element (FE) method with self-adaptive mesh-refinement technique is developed for solving the density functional Kohn–Sham equations. The FE method adopts local piecewise polynomials basis functions, which produces sparsely structured matrices of Hamiltonian. The method is well suitable for parallel implementation without using Fourier transform. In addition, the self-adaptive mesh-refinement technique can control the computational accuracy and efficiency with optimal mesh density in different regions.

1. Introduction

The density functional Kohn–Sham equation [1] has been widely used to calculate the electronic structure of materials. Various methods have been successfully developed to solve the Kohn–Sham equation, which can be divided into two categories according to the basis set adopted, i.e., the **k**-space and real space methods. The **k**-space methods use plane waves or atomic-like orbital to expand the Bloch wave functions, whereas the real-space methods directly solve the Kohn–Sham equation using the finite-difference (FD) [2–7] and finite-element (FE) [8–14] methods.

In the past decade, the method based on the combination of density functional theory and pseudopotential had been a very powerful tool for the calculation of electronic properties of materials. However, some difficulties are involved in **k**-space calculations. For instance, extensive global communications in dealing with plane waves reduce the efficiency of massive parallelization, which is necessary for complex systems. Meanwhile, usually generation of large super-cell is needed for non-periodic system, which certainly increases the computational cost. In contrast, the real-space method does not involve these problems, and has various advantages. The strictly local basis functions are essential for the order-N ($O(N)$) calculation. The arbitrary boundary conditions can easily be incorporated. Most importantly, the calculation including external field which breaks the translational symmetry can be easily performed. The real-space method does not use Fourier transforms, which produces sparsely structured Hamiltonian matrices necessary for parallel implementation.

FE method is a typical real-space method, using local piecewise polynomials basis functions. In addition, it is relatively straightforward for implementing adaptive refinement techniques to describe regions around nuclei or chemical bonds where the wave functions vary rapidly. Therefore, the computational accuracy and efficiency can be controlled by using adaptive meshes [15]. In this Letter, we show how the Kohn–Sham equation can be solved with the self-adaptive tetrahedra mesh based on the finite-element method.

The Letter is organized as following, in Section 2 we provide the application of FE method for numerically solving the Kohn–Sham equation. In Section 3 we discuss the details in finite-element calculations including matrix elements, potentials, electronic density, eigen-solver and error estimator. In Section 4 some numerical results are presented. Finally, Section 5 shows the conclusions.

2. Finite-element representation of Kohn–Sham equation

In the framework of the density functional theory (DFT) the minimization of the total energy is reached by the self-consistent solution of the Kohn–Sham equation [16–18]

$$\left[-\frac{1}{2}\nabla^2 + V_{\text{eff}}(\boldsymbol{r})\right]\psi_i(\boldsymbol{r}) = \epsilon_i\psi_i(\boldsymbol{r}), \tag{1}$$

* Corresponding author. Tel.: +86 21 65642679; fax: +86 21 65428369.
E-mail address: xggong@fudan.edu.cn (X.-G. Gong).

0375-9601/$ – see front matter
doi:10.1016/j.physleta.2008.05.075

$$V_{\text{eff}}(\boldsymbol{r}) = \sum_s V^s_{\text{ion}}(\boldsymbol{r} - \boldsymbol{R}^s) + V_{\text{Hartree}}(\boldsymbol{r}) + V_{\text{xc}}(\boldsymbol{r}) + V_{\text{ext}}(\boldsymbol{r}), \tag{2}$$

where the first, second, and third terms on the right side of Eq. (2) are the ionic pseudopotential, Hartree potential, and exchange-correlation potential respectively, while V_{ext} is the external potential.

The Hartree potential is the Coulomb interaction of electrons,

$$V_{\text{Hartree}}(\boldsymbol{r}) = \int \frac{\rho(\boldsymbol{r}')}{|\boldsymbol{r} - \boldsymbol{r}'|} d\boldsymbol{r}', \tag{3}$$

satisfying the Poisson equation

$$-\Delta V_{\text{Hartree}} = 4\pi\rho. \tag{4}$$

In numerical calculations the cost of solving the Poisson equation is far less than the integrals in Eq. (3).

The exchange-correlation potential is the functional of electronic density in local density approach (LDA),

$$E^{\text{LDA}}_{\text{xc}}[\rho] = \int d\boldsymbol{r}\, \rho(\boldsymbol{r}) \varepsilon_{\text{xc}}\big(\rho(\boldsymbol{r})\big), \tag{5}$$

$$V^{\text{LDA}}_{\text{xc}}(\boldsymbol{r}) \equiv \frac{\delta E^{\text{LDA}}_{\text{xc}}[\rho]}{\delta\rho(\boldsymbol{r})} = \varepsilon_{\text{xc}}\big(\rho(\boldsymbol{r})\big) + \rho(\boldsymbol{r}) \frac{d\varepsilon_{\text{xc}}(\rho(\boldsymbol{r}))}{d\rho(\boldsymbol{r})}. \tag{6}$$

Usually although several formulations of the exchange-correlation potentials are used [19], each of them is essentially the same for numerical calculations.

In finite element (FE) method the wave functions are expanded with the piecewise-polynomial basis functions $\{\varphi_j\}$ on a set of real space interpolation nodes,

$$\psi(\boldsymbol{r}) = \sum_j u_j \varphi_j. \tag{7}$$

The basis functions are typically chosen in such a way that φ_j is 1 on jth FE interpolation node while 0 on all the other nodes. As a result, the ith component of the wave function u_j is just the value of the wave function itself on each node. To find an approximate solution we discretize the equation within the subspace spanned by the basis functions. In this way, solving Eq. (1) is reduced to a generalized matrix eigenvalue problem determining the approximate eigenvalues ε and eigenfunctions u of the weak formulation [11]

$$Hu = \varepsilon S u, \tag{8}$$

where

$$H_{ij} = \frac{1}{2} \int_{\Omega} (\nabla\varphi_i \cdot \nabla\varphi_j)\, d\mathbf{r} + \int_{\Omega} \varphi_i V_{\text{eff}} \varphi_j\, d\mathbf{r}, \tag{9}$$

and

$$S_{ij} = \int_{\Omega} \varphi_i \varphi_j\, d\mathbf{r}. \tag{10}$$

Ω is a polygon domain which is divided into several tetrahedra. In Fig. 1 we sketch a 2-dimensional triangular mesh which is divided into triangles. In electronic calculations Ω can be a supercell for crystals or a large enough cuboid for finite systems. In present work we start with an initial regular 3-dimensional mesh consisting of many cubes, each of which is divided into 6 tetrahedra, as shown in Fig. 2. In our implementation the quadratic basis functions on tetrahedral mesh are employed. There are 10 interpolation nodes on each tetrahedron.

The self-adaptive mesh focus on the error of wave functions automatically. Here we generate a self-adaptive mesh for C_{60} which has more dense nodes near the atoms and bonding areas as shown in Fig. 3. These self-adaptive meshes are generated by an iteration of the mesh refinement, depending on the posterior error estimation [20]. The details of the error estimation will be described in Section 3.6.

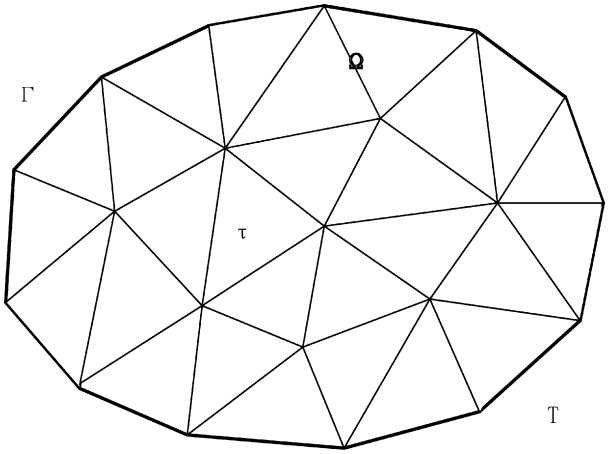

Fig. 1. 2D triangle mesh, Ω is a polygon domain with the border $\Gamma = \partial\Omega$, mesh $T = \{\tau\}$ is a triangle partition of Ω, τ denotes any triangle.

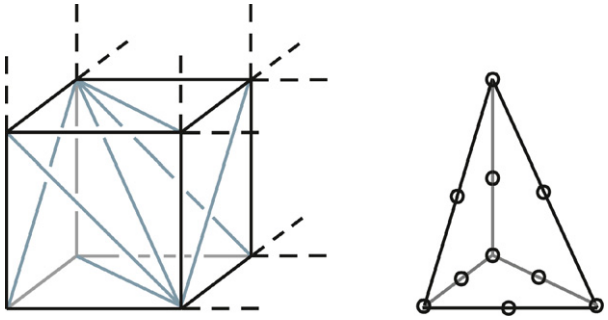

Fig. 2. A cube consisting of 6 tetrahedra. In the case of quadratic basis functions the FE interpolation nodes of one tetrahedra occupy the vertices and midpoints of edges.

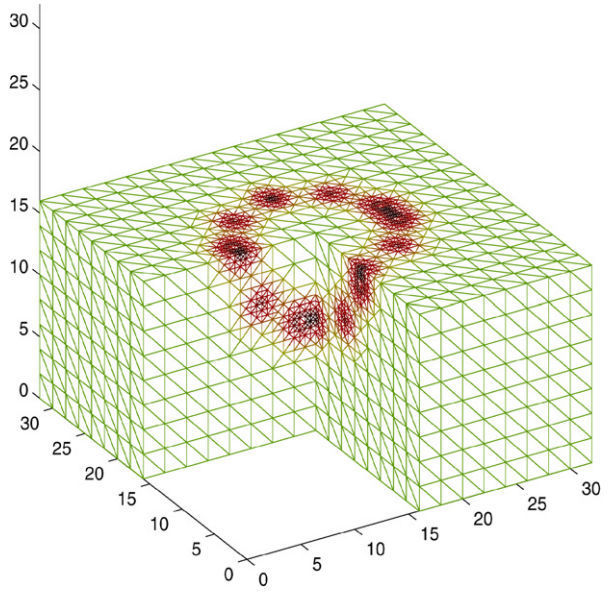

Fig. 3. The inner profile of an adaptive mesh generated for the calculation of C_{60}.

3. Finite-element calculation

3.1. Matrix generation

One advantage of FE method is that it produces sparse matrices shown in Fig. 4. To calculate the matrix elements we need to compute the following integrals on each tetrahedron τ

$$\int_\tau H_{ij}^{(\tau)} = \frac{1}{2}\int_\tau (\nabla\varphi_i \cdot \nabla\varphi_j)\,d\mathbf{r} + \int_\tau \varphi_i \hat{V}_{\text{eff}}\varphi_j\,d\mathbf{r}, \tag{11}$$

$$S_{ij}^{(\tau)} = \int_\tau \varphi_i\varphi_j\,d\mathbf{r}, \tag{12}$$

where φ_i and φ_j are the basis functions on the interpolation nodes of the tetrahedron τ. The global matrix H or S is the summation over all the local matrices $H^{(\tau)}$ or $S^{(\tau)}$ of tetrahedron τ,

$$H_{ij} = \sum_\tau H_{ij}^{(\tau)}, \qquad S_{ij} = \sum_\tau S_{ij}^{(\tau)}. \tag{13}$$

The local matrix $H^{(\tau)}$ or $S^{(\tau)}$ is a 10×10 matrix which is generated by the integration localized on tetrahedron τ.

The integrals over tetrahedron τ

$$\int_\tau f(x)\,dx \tag{14}$$

can be performed from the integral over standard tetrahedron $\hat{\tau}$.

$$\int_\tau f(x)\,dx = \left|\det(M_\tau)\right| \int_{\hat{\tau}} \hat{f}(\hat{x})\,d\hat{x}, \tag{15}$$

where M_τ is the transform matrix from the standard tetrahedron $\hat{\tau}$ to a general tetrahedron τ. Set the affine transformation $F_\tau : \hat{\tau} \to \tau$

$$F_\tau(\hat{x}) = M_\tau\hat{x} + b_\tau = x, \tag{16}$$

$$f(x) = f\big[F_\tau(\hat{x})\big] = \hat{f}(\hat{x}). \tag{17}$$

Generally Gaussian quadrature formulae can be used to approximately calculate the numerical integrals in the case that no analytical results are available. Over the standard tetrahedron $\hat{\tau}$ the integral can be approximately expressed as

$$\int_{\hat{\tau}} \hat{f}(\hat{x})\,d\hat{x} \approx \sum_{l=1}^{L} \hat{\omega}_l \hat{f}(\hat{b}_l), \tag{18}$$

where $\hat{\omega}_l$ is the weights, $\hat{b}_l \in \hat{\tau}$ is the Gaussian interpolation nodes.

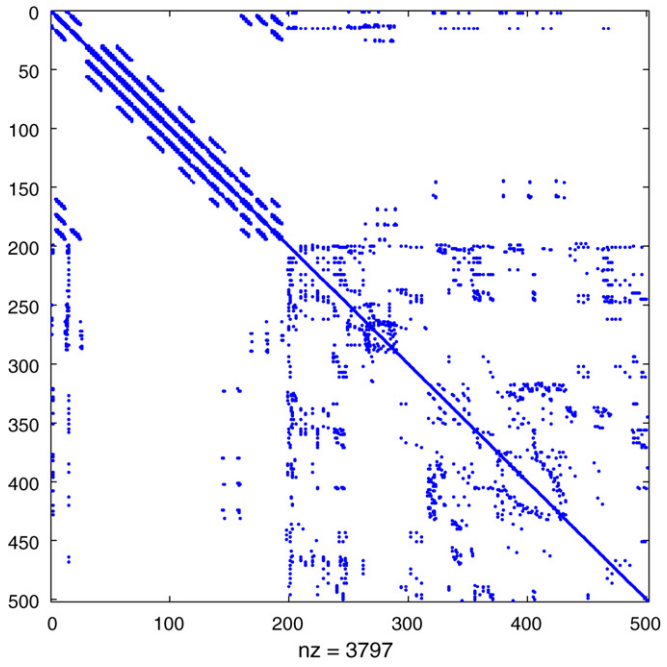

Fig. 4. Structure of a typical sparse matrix.

To speed up the computation we extract the analytic part of the integrals, which is computed with exact formula. As an example we consider the overlap matrix $S_{ij}^{(\tau)}$. With Eqs. (10) and (15) we get

$$S_{ij}^{(\tau)} = \left|\det(M_\tau)\right| \int_{\hat{\tau}} \hat{\varphi}_i(\hat{\mathbf{r}})\hat{\varphi}_j(\hat{\mathbf{r}})\,d\hat{\mathbf{r}}. \tag{19}$$

It is obvious that local matrices $S^{(\tau)}$ are similar to each other. More precisely they are the same except a different linear factor, that is, $S^{(\tau)}$ is the product of the standard local matrix $S^{(\hat{\tau})} = \int_{\hat{\tau}} \hat{\varphi}_i(\hat{\mathbf{r}})\hat{\varphi}_j(\hat{\mathbf{r}})\,d\hat{\mathbf{r}}$ and $|\det(M_\tau)|$ which is the volume determinant of the tetrahedron τ

$$\det(M_\tau) = \begin{vmatrix} x_1 & x_2 & x_3 & x_4 \\ y_1 & y_2 & y_3 & y_4 \\ z_1 & z_2 & z_3 & z_4 \\ 1 & 1 & 1 & 1 \end{vmatrix}. \tag{20}$$

The kinetic energy part and the Hartree potential can also be computed with exact formula which will be discussed in the following sections separately. However for the other parts of the integrals, the ionic potential and exchange-correlation potential, no analytic expression is available, therefore numerical approximation must be adopted.

3.2. The kinetic operator

The integral of kinetic energy part of the $H_{ij}^{(\tau)}$ is the matrix element of Laplace operator T, which can also be written in analytic form,

$$\begin{aligned} T_{ij}^{(\tau)} &= \frac{1}{2}\int_\tau (\nabla\varphi_i \cdot \nabla\varphi_j)\,d\mathbf{r} \\ &= \frac{1}{2}\int_\tau \sum_{kl} \frac{\partial\varphi_i}{\partial\lambda_k}\frac{\partial\varphi_j}{\partial\lambda_l}\nabla\lambda_k \cdot \nabla\lambda_l\,d\mathbf{r}. \end{aligned} \tag{21}$$

The global kinetic energy matrix T is the summation over all the local $T^{(\tau)}$,

$$T_{ij} = \sum_\tau T_{ij}^{(\tau)}. \tag{22}$$

Due to the invariance of the Laplace operator under rotation and translation it can be proved that the local kinetic energy matrix $T^{(\tau)}$ is also invariant under such transformations.

Lemma 1. *For the congruent tetrahedra τ and τ' the corresponding local kinetic energy matrices are exactly the same*

$$T^{(\tau)} = T^{(\tau')}. \tag{23}$$

Proof. Set the affine transformation $F : \tau \to \tau'$

$$F_\tau(x) = Q_\tau x + b_\tau = x', \tag{24}$$

where Q is an orthogonal matrix if the tetrahedra τ and τ' are congruent. Therefore

$$\begin{aligned} T_{ij}^{(\tau)} &= \int_\tau (\nabla\varphi_i)^T \cdot (\nabla\varphi_j)\,d\mathbf{r} \\ &= \frac{1}{\det(Q)}\int_{\tau'} (Q\,\nabla'\varphi_i')^T \cdot (Q\,\nabla'\varphi_j')\,d\mathbf{r}' \\ &= \int_{\tau'} (\nabla'\varphi_i')^T \cdot (\nabla'\varphi_j')\,d\mathbf{r}' = T_{ij}^{(\tau')}. \qquad \square \end{aligned} \tag{25}$$

Lemma 2. *With a linear transformation* $F:\tau\to\tau'$

$$F(x)=\alpha Ix=x',\quad \alpha>0, \tag{26}$$

the local kinetic energy matrices are linearly related

$$\alpha T^{(\tau)}=T^{(\tau')}. \tag{27}$$

Proof.

$$\begin{aligned}T_{ij}^{(\tau)}&=\int_{\tau}(\nabla\varphi_i)^T\cdot(\nabla\varphi_j)\,d\mathbf{r}\\&=\frac{\alpha^2}{\det(\alpha I)}\int_{\tau'}(\nabla'\varphi_i')^T\cdot(\nabla'\varphi_j')\,d\mathbf{r}'\\&=\frac{1}{\alpha}\int_{\tau'}(\nabla'\varphi_i')^T\cdot(\nabla'\varphi_j')\,d\mathbf{r}'=\frac{1}{\alpha}T_{ij}^{(\tau')}.\end{aligned}\quad\square \tag{28}$$

The present refinement method with initial regular mesh results in only 3 types of tetrahedron as shown in Fig. 5, and tetrahedra of same type are congruent with each other [15]. Therefore only 3 types of typical local kinetic energy matrix need to be calculated. All the other local kinetic matrices can be obtained by the linear transformation from these 3 types. We refer them hereafter as standard types.

3.3. Hartree potentials

For the potential part, present method is also applicable in some cases. For example we get the Hartree potential by solving the Poisson equation

$$-\Delta V_{\text{Hatree}}=4\pi\rho, \tag{29}$$

which is discretized on the same FE subspace and reduced to linear algebraic equations

$$Tv=f, \tag{30}$$

where T is the Laplace operator and f is the right-hand vector

$$f_i=2\pi\int_{\Omega}\rho\varphi_i\,d\mathbf{r}. \tag{31}$$

The calculation of the electronic density ρ will be described in Section 3.5.

Solving Eq. (30) leads to the discretized formula of Hartree potential.

$$V_H(\mathbf{r})=\sum_{i=1}^{n}v_{H,i}\varphi_i(\mathbf{r})\quad(\mathbf{r}\in\Omega). \tag{32}$$

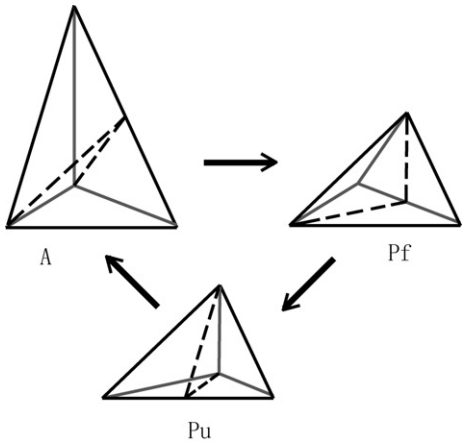

Fig. 5. 3 standard types of tetrahedron.

The integrals of $\varphi_iV_H(\mathbf{r})\varphi_j$ over each tetrahedron τ can be written in analytic form

$$\begin{aligned}\int_{\tau}\varphi_iV_H(\mathbf{r})\varphi_j\,d\mathbf{r}&=\int_{\tau}\varphi_i\varphi_j\sum_k v_{H,k}\varphi_k\,d\mathbf{r}\\&=\sum_k V_{H,k}\int_{\tau}\varphi_i\varphi_j\varphi_k\,d\mathbf{r}\\&=\det(M_\tau)\sum_k v_{H,k}\int_{\hat\tau}\hat\varphi_i\hat\varphi_j\hat\varphi_k\,d\hat{\mathbf{r}}.\end{aligned} \tag{33}$$

3.4. Nonlocal part of the pseudopotential

Another issue concerns the non-locality of the ionic pseudopotentials. In FE the local basis functions produce sparse matrices, but the non-localization of the angular momentum operator in norm-conserving pseudopotentials [21] destroys the localization of the operators and produces full matrix. To present the sparse form of pseudopotentials we employ the Kleinman–Bylander pseudopotential [22],

$$\hat V^{ps}=V_{\text{loc}}(r)+\sum_{l=0}^{L}\sum_{m=-l}^{+l}\frac{|V_l(r)\psi_{lm}^{ps}(r,\theta,\phi)\rangle\langle\psi_{lm}^{ps}(r,\theta,\phi)V_l(r)|}{\langle\psi_{lm}^{ps}(r,\theta,\phi)|V_l(r)|\psi_{lm}^{ps}(r,\theta,\phi)\rangle}, \tag{34}$$

where $\psi_{lm}^{ps}(r,\theta,\phi)$ is the pseudo-wave-function of atom.

The second term in the right side of Eq. (34) is a nonlocal one. Let matrix $\mathbf{A}$ be the discretization of this nonlocal part, we have

$$A_{ij}=\sum_{l=0}^{L}\sum_{m=-l}^{+l}\frac{\langle\varphi_i|V_l(r)\psi_{lm}^{ps}(r,\theta,\phi)\rangle\langle\psi_{lm}^{ps}(r,\theta,\phi)V_l(r)|\varphi_j\rangle}{\langle\psi_{lm}^{ps}(r,\theta,\phi)|V_l(r)|\psi_{lm}^{ps}(r,\theta,\phi)\rangle}. \tag{35}$$

For the sake of simplicity we define vector $\mathbf{C}_{lm}$

$$C_{lm,i}=\langle\varphi_i|V_l(r)\psi_{lm}^{ps}(r,\theta,\phi)\rangle, \tag{36}$$

and

$$\upsilon_{lm}=\frac{1}{\langle\psi_{lm}^{ps}(r,\theta,\phi)|V_l(r)|\psi_{lm}^{ps}(r,\theta,\phi)\rangle}. \tag{37}$$

Therefore

$$A_{ij}=\sum_{l=0}^{L}\sum_{m=-l}^{+l}C_{lm,i}\upsilon_{lm}C_{lm,j}. \tag{38}$$

The full matrix $\mathbf{A}$ can be expressed as follows

$$\mathbf{A}=\sum_{l=0}^{L}\sum_{m=-l}^{+l}\mathbf{C}_{lm}\upsilon_{lm}\mathbf{C}_{lm}^T=\mathbf{CVC}^T, \tag{39}$$

where

$$\mathbf{C}=(\mathbf{C}_{lm}), \tag{40}$$

$$\mathbf{V}=\operatorname{diag}(\upsilon_{lm}). \tag{41}$$

$\mathbf{A}$ is a product of matrices consisting of $((L+1)^2)$ vectors. For a full matrix the vectors $\mathbf{C}_{lm}$ need only $O(N\times(L+1)^2)$ memories instead of $O(N\times N)$.

3.5. The electronic density

The electronic density can be calculated from the wave functions

$$\rho(\mathbf{r})=\sum_k^M n_k\left|\psi_k(\mathbf{r})\right|^2, \tag{42}$$

where n_k is the occupation number of state k. The wave functions are separated on FE space by

$$\psi_k = \sum_{i=0}^{n} \psi_k(z_i)\varphi_i. \tag{43}$$

From above two equations,

$$\rho = 2\sum_{k}^{M} n_k \sum_{i,j=0}^{n} \psi_k(z_i)\psi_k(z_j)\varphi_i\varphi_j. \tag{44}$$

It is worthwhile to note that the electronic density cannot be represented by the same basis of the wave functions. Obviously

$$\rho \neq 2\sum_{k}^{M} n_k \sum_{i=0}^{n} \left|\psi_k(z_i)\right|^2 \varphi_i. \tag{45}$$

The electronic density cannot be expanded by the components on FE interpolation nodes.

Eq. (44) can be rewritten as

$$\rho = \sum_{i,j=0}^{n} \rho_{ij}\varphi_i\varphi_j, \tag{46}$$

where

$$\rho_{ij} = 2\sum_{k}^{M} n_k \psi_k(z_i)\psi_k(z_j). \tag{47}$$

The density matrix ρ_{ij} is a full matrix which spends the storage of the scale $O(N^2)$. However we need not to store the whole density matrix. Because of the localization of the FE basis functions, most terms in Eq. (44) are zero. The non-zeros parts result in a sparse matrix

$$\tilde{\rho}_{ij} = \begin{cases} \rho_{ij}, & z_i, z_j \text{ in one tetrahedron,} \\ 0, & z_i, z_j \text{ not in one tetrahedron.} \end{cases} \tag{48}$$

The memory requirement for the sparse matrix $\tilde{\rho}$ is only of the scale $O(N)$ rather then $O(N^2)$.

3.6. Posterior error estimation for the mesh refinement

Generally, the numerical accuracy depends on the mesh density. Therefore the overall accuracy of the numerical approximation is deteriorated by local vibration of the wave functions or the potentials. Compared with the distant regions from the atom the regions around the atomic nuclei and between atoms of chemical bonds are more important. We have arranged more interpolation nodes in these regions. A practical technique is to refine the mesh near such critical regions, i.e., to place more nodes where the solution is less regular. We have adopted the self-adaptive method based on posterior-error analysis. Such a method focuses on the error of wave functions automatically and preserves the shape regularity for tetrahedral meshes during the refinement process.

In the present method, we use the gradient averaging technique to access posterior-error [24] for eigenvalue problems. As an example Fig. 6 shows a refined mesh. It can be seen that the mesh meets the error distribution.

3.7. Self-consistent of solving the Kohn–Sham equation

The present method of solving the Kohn–Sham equation is sketched in the following.

1. Generation of initial mesh.
2. Self-consistent calculation of the Kohn–Sham equation:
   (2.1) Initialize electronic density;
   (2.2) Calculate the effective potential;
   (2.3) Solve the eigenvalue problem;
   (2.4) Calculate new electronic density;
   (2.5) Go back to Step (2.2) if not convergent.
3. If the error posterior-estimated is not small enough, refine the mesh and go back to Step 2.

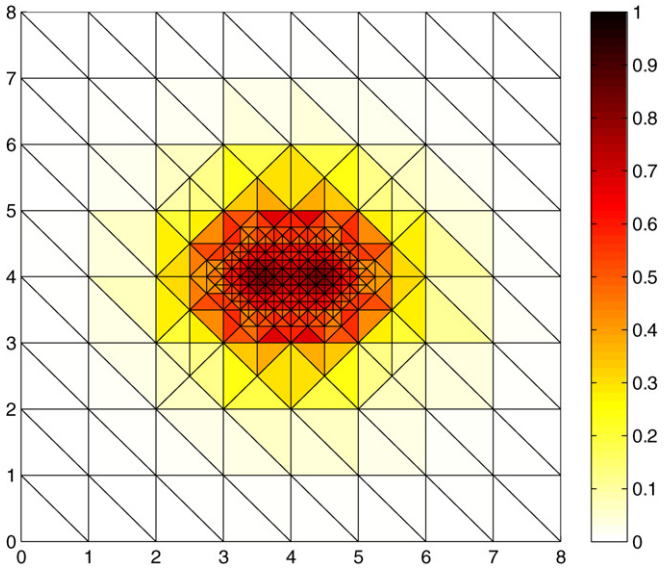

Fig. 6. The posterior-error distribution of H_2.

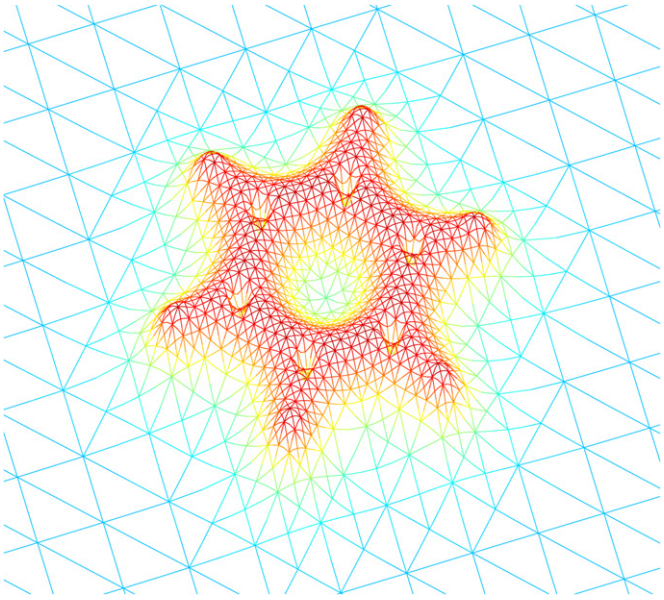

Fig. 7. Electronic density of C_6H_6 (benzene) on x–y plane.

Two nested iterations, i.e. outer iteration and inner iteration are designed in our code. The outer iteration is the mesh refinement for the accuracy required. The loop refines mesh till the accuracy requirement is satisfied. The inner iteration deals with the self-consistent field (SCF) solutions for the Kohn–Sham equation.

In step (2.3) we employed LOBPCG method [23] to solve the eigenvalue problem (8). In step (2.4) we employed Broyden method [25–27] for charge mixing. The initial electronic density in step (2.1) is determined by the interpolation from results on coarse mesh points. Therefore the SCF iteration can operate continuously during the mesh refinement.

Table 1
Results for some molecule systems

	Error estimation	Refinement time	FE nodes	Bonding energy (eV)	
				Present work	VASP result
H_2	1.0×10^{-5}	13	5763	6.69	6.70
	5.0×10^{-5}	11	3698	6.69	
CH_4	1.0×10^{-5}	16	13275	24.86	24.87
	5.0×10^{-5}	13	5865	24.81	
C_2H_2	1.0×10^{-5}	16	22951	24.21	24.19
	5.0×10^{-5}	13	7924	24.18	
C_6H_6	1.0×10^{-5}	15	25492	80.96	80.95
	5.0×10^{-5}	13	13305	80.39	
$C_{13}H_9$	1.0×10^{-5}	15	39101	160.25	160.78
	5.0×10^{-5}	13	19224	159.10	
Al_4	1.0×10^{-6}	14	20283	7.26	7.33
	1.0×10^{-5}	10	5328	7.20	

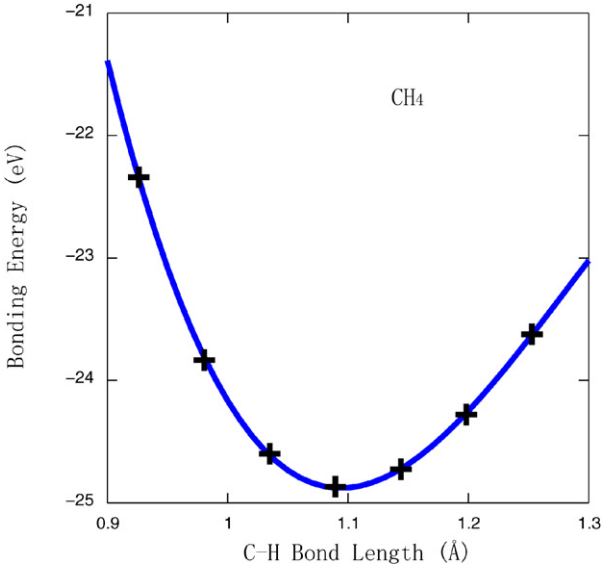

Fig. 8. Calculated C–H bonding energy versus bond length for CH_4.

4. Numerical test

In order to show the efficiency of our method, we have calculated the electronic structure of several molecules. Local Density Approximation (LDA) by Perdew/Zunger '81 [28] is adopted as the exchange-correlation potential and the normal-conserving pseudopotential is generated by the package **fhi98PP**. The results are listed in Table 1. The electronic density of C_6H_6 and the refined mesh is shown in Fig. 7. It can be clearly seen that the present results are in close agreement with that from VASP code, which indicates that the present FE method works.

We have calculated the C–H bonding energy versus bond length of CH_4, the result is shown in Fig. 8. The calculated equilibrium C–H bond length is 1.094 Å, in a good agreement with the experiment result (1.09 Å).

5. Summary

The FE method based on self-adaptive mesh refinement for solving Kohn–Sham equations is presented. This approach combines the advantages of FE method with adaptive tetrahedral mesh to reduce the calculations. The method is implemented on distributed parallel computation, which is a promising method for first principle study of large system.

Acknowledgements

The authors deeply thanks to Wei-Guo Gao, Lin-bo Zhang, Lin-Wang Wang, Eiji Tsuchida, Ping-Wen Zhang, Xiao-Ying Dai, Xiao Gu, Min Ji, Xiao-Hua Zhang, Guo-Wu Ren, Mei-Yue Shao and Bin Wang. This work is partially supported by the National Basic Research Program of China (973 Program), MOE and NSF of China.

References

[1] W. Kohn, L.J. Sham, Phys. Rev. 140 (1965) A1133.
[2] J. Wang, T.L. Beck, J. Chem. Phys. 112 (2000) 9223.
[3] J.R. Chelikowsky, N. Troullier, Y. Saad, Phys. Rev. Lett. 72 (1994) 1240.
[4] K. Hirose, T. Ono, Y. Fujimoto, S. Tsukamoto, First-Principles Claculations in Real-Space Formalism, Imperial College Press, 2005, p. 1.
[5] F. Gygi, G. Galli, Phys. Rev. B 52 (1995) R2229.
[6] E.L. Briggs, D.J. Sullivan, J. Bernholc, Phys. Rev. B 54 (1996) 14362.
[7] N.A. Modine, G. Zumbach, E. Kaxiras, Phys. Rev. B 55 (1997) 10289.
[8] E. Tsuchida, M. Tsuukada, Phys. Rev. B 52 (1995) 5573.
[9] E. Tsuchida, M. Tsuukada, Phys. Rev. B 54 (1996) 7602.
[10] E. Tsuchida, M. Tesukada, J. Phys. Soc. Jpn. 67 (1998) 3844.
[11] J.E. Pask, B.M. Klein, P.A. Sterne, C.Y. Fong, Comput. Phys. Commun. 135 (2001) 1.
[12] E. Tsuchida, J. Chem. Phys. 121 (2004) 4740.
[13] J.E. Pask, P.A. Sterne, Model. Simul. Mater. Sci. Eng. 13 (2005) R7.
[14] T. Torsti, T. Eirola, J. Enkovaara, T. Hakala, P. Havu, V. Havu, T. Höynälänmaa, J. Ignatius, M. Lyly, I. Makkonen, T.T. Rantala, J. Ruokolainen, K. Ruotsalainen, E. Räsänen, H. Saarikoski, M.J. Puska, Phys. Status Solidi B 243 (2006) 1016.
[15] D. Zhang, A. Zhou, X.G. Gong, Commun. Comput. Phys., in press.
[16] W. Kohn, Rev. Mod. Phys. 71 (1999) 1253.
[17] R.O. Jones, O. Gunnarsson, Phys. Rev. Lett. 55 (1985) 107.
[18] M.R. Martin, Electronic Structure, Cambridge Univ. Press, 2004.
[19] M.E. Casida, in: J.M. Seminario (Ed.), Recent Developments and Applications of Modern Density Functional Theory, Elsevier, Amsterdam, 1996.
[20] M. Ainsworth, J.T. Oden, Wiley, 2000.
[21] D.R. Hamann, M. Schlüter, C. Chiang, Phys. Rev. Lett. 43 (1979) 1494.
[22] L. Kleinman, D.M. Bylander, Phys. Rev. Lett. 48 (1982) 1425.
[23] A. Knyazev, SIAM J. Sci. Comput. 23 (2001) 517.
[24] D. Mao, L. Shen, A. Zhou, Adv. Comput. Math. 25 (1–3) (2006) 135.
[25] C.G. Broyden, Math. Comput. 19 (1965) 577.
[26] G.P. Srivastava, J. Phys. A 17 (1984) L317.
[27] D.D. Johnson, Phys. Rev. B 38 (1988) 12807.
[28] J.P. Perdew, A. Zunger, Phys. Rev. B 23 (1981) 5048.